Current Biology *16*, 767–772, April 18, 2006 ©2006 Elsevier Ltd All rights reserved DOI 10.1016/j.cub.2006.02.069

Report

Octopuses Use a Human-like Strategy to Control Precise Point-to-Point Arm Movements

Germán Sumbre,[1,4] Graziano Fiorito,[2] Tamar Flash,[3] and Binyamin Hochner[1,*]

[1] Department of Neurobiology and Interdisciplinary Center for Neuronal Computation Institute of Life Sciences Hebrew University Jerusalem 91904 Israel

[2] Laboratorio di Neurobiologia Stazione Zoologica "Anton Dohrn" di Napoli Naples 80121 Italy

[3] Department of Computer Science and Applied Mathematics Weizmann Institute of Science Rehovot 76100 Israel

Summary

One of the key problems in motor control is mastering or reducing the number of degrees of freedom (DOFs) through coordination [1]. This problem is especially prominent with hyper-redundant limbs such as the extremely flexible arm of the octopus [2]. Several strategies for simplifying these control problems have been suggested for human point-to-point arm movements [3–6]. Despite the evolutionary gap and morphological differences, humans and octopuses evolved similar strategies when fetching food to the mouth. To achieve this precise point-to-point-task, octopus arms generate a quasi-articulated structure based on three dynamic joints. A rotational movement around these joints brings the object to the mouth [7]. Here, we describe a peripheral neural mechanism—two waves of muscle activation propagate toward each other, and their collision point sets the medial-joint location. This is a remarkably simple mechanism for adjusting the length of the segments according to where the object is grasped. Furthermore, similar to certain human arm movements, kinematic invariants were observed at the joint level rather than at the end-effector level, suggesting intrinsic control coordination. The evolutionary convergence to similar geometrical and kinematic features suggests that a kinematically constrained articulated limb controlled at the level of joint space is the optimal solution for precise point-to-point movements.

*Correspondence: bennyh@lobster.ls.huji.ac.il

[4] Present address: Division of Neurobiology, Department of Molecular and Cell Biology, University of California, Berkeley, Berkeley, California 94720.

Results and Discussion

The Fetching Movement Is Executed Mainly by Rotation of the Medial Joint

Octopuses reach out to catch food by first extending an arm to grasp the food with their suckers. Then, in order to fetch the food to the mouth, the arm generates a series of bends that function as proximal, medial, and distal joints (Figure 1). The fetching movements are generated by rotating the segments formed around the joints (Figure 1 and Figure S3 in the Supplemental Data available with this article online). In 24 fetching movements from five octopuses analyzed in detail, the medial joint (θ_2) showed the most robust behavior, manifested as a large rotation (average ± standard deviation [SD], 100.1° ± 8°, Figure S3B) with relatively low variance among movements (Figure S3D, yellow). The proximal joint (θ_1) performed smaller rotations (average ± SD, 11.6° ± 11°, Figure S3A) but still with a relatively low variance (Figure S3D, blue). In all 24 movements analyzed, the angle of the medial joint (θ_2) increased throughout the entire movement (Figure S3B). In 16 of the 24 movements, the angle of the proximal joint (θ_1) clearly first decreased and then increased (blue), whereas in the other eight movements, the angle only decreased (red). The movement of the medial joint (θ_2) therefore appears to account for most of the movement, whereas the degree of coordination between the medial and proximal joints (θ_1) determines the distal-joint path. In contrast to these two joint rotations, the angular rotation of the distal joint (θ_3) (average ± SD, 37.9° ± 27°, Figure S3C) was highly variable (Figure S3D, green). This suggests that the distal joint plays a significant role only during the last phase of the fetching movement, when the distal joint rotates to bring the food to the mouth (data not shown).

At What Level Is the Fetching Movement Controlled?

Studies in humans suggest that the control of arm movements may be represented either in terms of intrinsic or extrinsic (extracorporeal) coordinates [8]. To determine how the octopus controls fetching movements, we looked for invariant relationships among the joint angular rotations or for invariant paths expressed in terms of external Cartesian coordinates of the food and the distal-joint locations (n = 24, from five animals). When plotting the relationship between joint angles (θ_1 and θ_2), we found that movements could be classified into two different groups by computing a curvature function of the curve describing the relationship between the joint angles (see Supplemental Experimental Procedures).

Movements in the first group (Figure 2A) showed simple negative linear correlations between the time-dependent angular rotations of θ_1 and θ_2 (n = 8, average ± SD, $R^2 = 0.99 \pm 0.001$, ($p < 7 \times 10^{-6}$ for all movements (F test); $\alpha = 0.05$ for all the following statistical tests). The average slope ± SD for these curves was -18.72 deg^2 ± 17.51 deg^2. Movements belonging to the second group (Figures 2B and 2C) showed

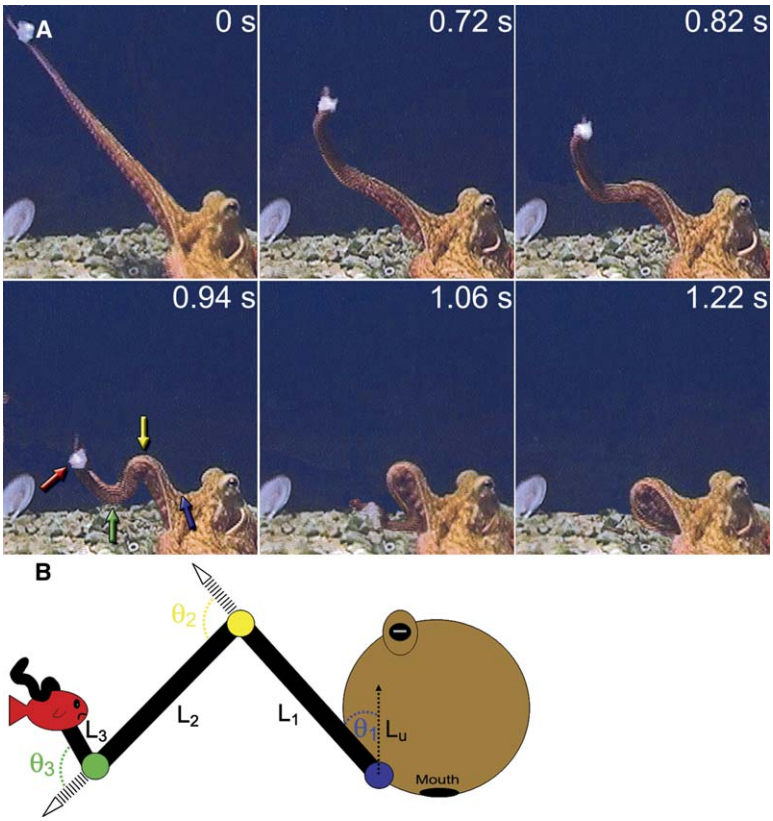

Figure 1. Octopus Fetching Movements Involve a Quasi-Articulated Structure of the Arm

(A) A sequence of six video images at times indicated during a fetching movement. Red arrow marks location of the food. Green, yellow, and blue arrows, respectively, mark the distal, medial, and proximal bends.

(B) A schema of the quasi-articulated structure with the nomenclature for the joints and segments used in the text.

a relationship between the time-dependent angular rotations of θ_1 and θ_2, which could be described by two nearly straight lines separated by an abrupt change in slope. The average slope for the first segment was $-41.45\ deg^2 \pm 42.88\ deg^2$ (n = 16, with averaged R^2 = 0.99 ± 0.009, $p < 5 \times 10^{-4}$ for all movements [F test]), and the averaged slope for the second segment was $-34.12\ deg^2 \pm 125.94\ deg^2$ (n = 16, with averaged R^2 = 0.97 ± 0.03, ($p < 0.008$ for all movements [F test]).

Describing the spatial paths of the food and of the distal joint in terms of their Cartesian coordinates revealed that these paths could be classified as being either moderately straight (Figure 2F) or as having a complex form that did not follow any specific pattern (Figures 2D and

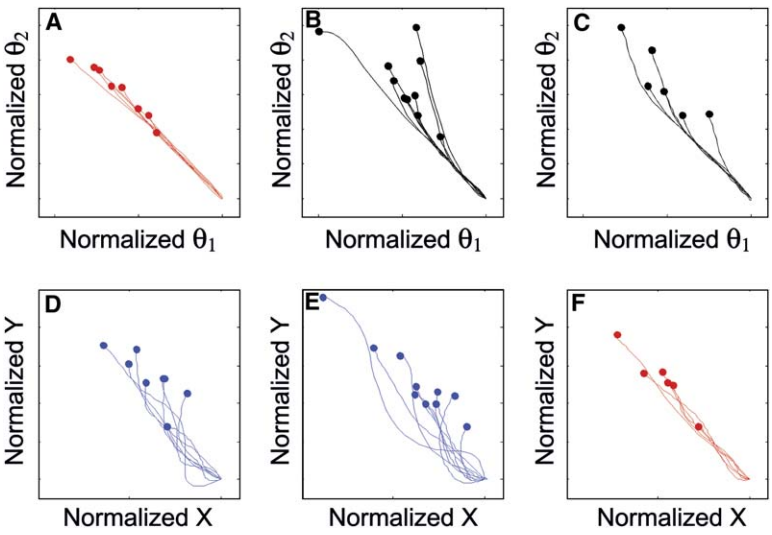

Figure 2. The Fetching Movements Are Controlled in Intrinsic Coordinates

(A) The relationship between the proximal-joint (θ_1) and the medial-joint (θ_2) rotations of the fetching movements belonging to the first group is represented by a single linear segment.

(B) As in (A), for movements that belong to the second group (two linear segments with different slopes) and show complex relationships in Cartesian coordinates (shown in [E]).

(C) As in (B), for movements that belong to the second group and show linear relationships in Cartesian coordinates (shown in [F]).

(D) The paths described by the distal joint within the best-fitted plane, showing more curved paths in spatial coordinates and belonging to the single-linear-curve group in joint space (shown in [A]).

(E) As in (D), but movements that belong to the two-linear-segment group in joint space (shown in [B]).

(F) The paths described by the distal joint within the best-fitted plane, showing a linear path in Cartesian coordinates and belonging to the two-linear-segment group in joint space (shown in [C]).

All curves were shifted to the same starting position and rotated to −45°, n = 24. For clarity, linear relationships are colored in red, relationships based on two linear segments are in black, and complex curves are in blue. The end of each curve is indicated by a small dot in the respective color.

2E); their curvature function showed multiple short and wide peaks (see Supplemental Experimental Procedures). The food paths that showed moderately straight curves (n = 7) had an average $R^2 = 0.97 \pm 0.02$, ($p < 5 \times 10^{-5}$ for all movements [F test]); in contrast, the more curved paths of the food (n = 17) yielded averaged $R^2 = 0.57 \pm 0.32$, ($p < 0.02$ for 15 out of 18 movements [F test]). The paths of the distal joint of the moderately straight group (Figure 2F, n = 6) showed average $R^2 = 0.98 \pm 0.01$, ($p < 7 \times 10^{-7}$ for all movements [F test]), and those following more curved paths (Figures 2D and 2E) showed average $R^2 = 0.55 \pm 0.27$, ($p < 0.038$ for 17 out of 18 movements [F test]). For a summary of the statistical results, see Table S4.

In summary, straight lines fitted to the curves described by the relationship between joint rotations had significantly higher R^2 values (for each of the linear segments) than those describing the spatial paths in terms of Cartesian coordinates of either the food or of the distal joint ($p = 8 \times 10^{-8}$ and $p = 10^{-9}$, respectively [two-tailed t test]). In addition, the curves describing the relationships between the normalized joint angles showed an averaged variance among movements of 0.028 ± 0.002, whereas the averaged variance among movements for normalized distal-joint paths described in normalized Cartesian coordinates was 0.052 ± 0.027; and 0.072 ± 0.026, among food paths. The variance among curves describing the relationship between joint angles was significantly smaller than both the variance among the distal-joint paths ($p = 2 \times 10^{-16}$ [two-tailed t test]) and among the food paths ($p = 2.4 \times 10^{-7}$ [two-tailed t test]). Therefore, the well-coordinated pattern between joints suggests that octopuses control the fetching movements in terms of intrinsic coordinates [9–14].

Nonetheless, given that 25% of the movements showed linear correlations in Cartesian coordinates, control in extracorporeal coordinates cannot be completely ruled out. This type of control could be used for specific types of movements. For example, we found that 75% of the movements that followed a single linear segment in joint space (Figure 2A) were performed in the horizontal plane, and 83% of the movements following linear paths in extrinsic coordinates (Figure 2F) were performed within the vertical plane (above 45° with respect to the bottom of the aquarium). For an interesting analogy to human movements, see [15] and [16].

Figures 3A and 3B show individual examples of the two joint-space strategies described above. Figures 3C and 3D show the angular-velocity profiles for the proximal (blue) and medial (yellow) joints, corresponding to the respective movements in Figures 3A and 3B. In most cases, these profiles were bell-shaped with either a single (e.g., Figure 3C) or a double peak (e.g., Figure 3D) (for details, see Supplemental Data and [8]). Figures 3E and 3F show the paths of the distal joint (green) and of the medial joint (yellow) within the plane best fitting the movement. In Figure 3E, the distal joint shows a curved path (green), and the medial joint shows a simple linear path (yellow). In contrast, in Figure 3F, the distal joint (green) follows a more complex path, and the path of the medial joint (yellow) reverses its direction. The point in time when the direction of the joint rotation reversed (i.e., when the joint began to rotate in the opposite direction, as depicted by the yellow dotted line in Figure 3F) coincided with the abrupt change in the slope of the θ_2 versus θ_1 relationship (Figure 3B) and also with the minimum of the medial-joint angular-velocity profile (Figure 3D, dotted line). This hints that these movements are the product of two submovements (see Supplemental Data for details). These two motion-control strategies in joint space are not specific to a particular animal because four of the five octopuses whose movements were analyzed used these two joint-space strategies to generate fetching movements.

When the degree of linearity of the movement paths was correlated with the two types of relationships observed between the time-dependent θ_1 and θ_2 angular rotations, we found that movements belonging to the first group, which followed a linear joint-interpolation motion scheme (Figures 2A and 3A), showed a narrow range of values of index of linearity (see Supplemental Experimental Procedures) (0.092–0.211, n = 8) (Figure 3G). Movements belonging to the two-segment scheme (Figures 2B, 2C, and 3B) had a much broader range of values of the index of linearity (0.007–0.367, n = 16, Figure 3H) showing straighter paths, (Figure 2F) resulting in fetching movements that follow the shortest path to the mouth, as well as more complex curved paths (Figure 2E) that may be used to avoid external obstacles.

Neuromuscular Control

To gain insight into the control mechanisms underlying the generation of the arm's quasi-articulated structure, we recorded electromyograms (EMGs) at different locations along the arm and analyzed the spatiotemporal patterns of muscle activities during fetching movements (n = 58, from ten animals). Two electrodes were inserted at different positions along the arm. The sign of the delay between the onsets of the EMG signals recorded by the two electrodes depended on which segment the electrodes were recording from. When the two electrodes were situated within the proximal segment (L_1), the histogram of the normalized delay in the EMG onsets was distributed around a positive mean (0.08 ± 0.08 s/cm, n = 18, Figure 4A), indicating that the EMG signal propagated from the proximal toward the distal electrode.

In Figure 4B, the electrodes were located on either side of the medial joint; the histogram was distributed around a mean of 0.0 ± 0.08 s/cm (n = 19), significantly smaller than the mean in Figure 4A ($p = 0.004$, two-tailed t test). In Figure 4C, the electrodes recorded from the medial segment (L_2), and the onset delays were distributed around a negative value (-0.05 ± 0.05 s/cm, n = 21), significantly smaller than the mean in Figures 4A and 4C ($p = 10^{-7}$ and $p = 0.005$, two-tailed t test, respectively). Thus, the muscle activity propagated in the distal-to-proximal direction along the medial segment.

Similar tendencies for the delays between the onsets of the EMG signals at the two electrodes were obtained when different algorithms were used to calculate these onsets (Table S2). In addition, the delays between the onset of the EMG signals and the onset of the medial-joint formation show a positive mean, regardless of the segment in which the electrodes were inserted (proximal segment: 0.11 ± 0.17 s [n = 29] and distal segment: 0.09 ± 0.12 s [n = 29]). Both groups had means significantly larger than zero ($p = 7.5 \times 10^{-4}$ and $p = 10^{-4}$,

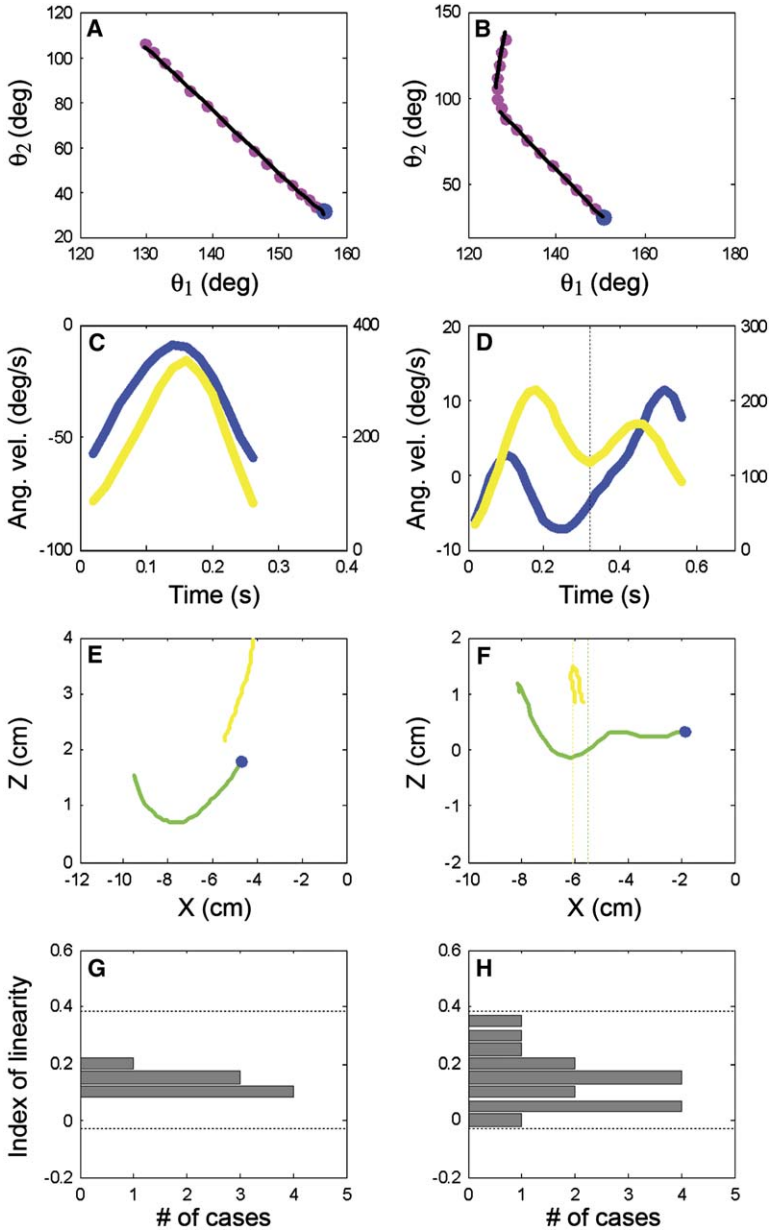

Figure 3. The Joint Space Control Can Be Classified into Two Different Strategies

(A) An example of a single-linear-segment curve with a negative slope representing the relationship between the proximal-joint (θ_1) and the medial-joint (θ_2) rotations of movements in the first group.

(B) An example of a curve based on two linear segments of different slopes, typical for movements in the second group. The magenta dots represent the digitized data, the black lines are the fitted straight lines, and the large blue dots give the movements' starting points.

(C and D) The angular-velocity profiles of θ_1 (blue) and θ_2 (yellow) calculated for the movements in (A) and (B), respectively. The vertical black dotted line in (D) shows the time of the abrupt slope change observed in (B).

(E and F) The paths of the distal (green) and the proximal joint (yellow) within the best-fitted plane for the movements in (A) and (B), respectively. The dashed vertical lines represent the time point of the abrupt change in slope in (B) for the path of the distal (blue) and the medial joint (yellow). The blue dot represents the end of the distal-joint path.

(G) The index of linearity histogram of the distal-joint path for movements classified as obeying the linear joint-interpolation motion-control scheme shown in (A), n = 8.

(H) As in (G), for movements obeying the second motor control scheme, which describes the time-dependent relationship between θ_1 and θ_2 by two nearly straight lines of different slopes as shown in (B), n = 16.

respectively [paired t test]) but not significantly different from each other (p = 0.69 [two-tailed t test]; Figure 4D and 4E). Medial-joint formation thus follows the onset of muscle activation on both sides of the joint.

These results suggest that the formation of the quasi-articulated structure involves two muscular-contraction waves that propagate in opposite directions toward each other. One wave starts at the base of the arm, and the second one begins at the distal joint or distally to it. Presumably, these two waves stiffen the quasi-articulated structure, and the pattern of muscle activation responsible for the medial-joint formation and rotation is generated or initiated around their collision point.

Motor Control Strategies

Human arm movements are represented in either hand (end-point) or joint space, depending on the task being executed [17–21]. In contrast, the octopus first controls the formation of the dynamic quasi-articulated structure in a space unique to flexible arms, namely limb configuration space. The octopus uses this space to dynamically adjust the lengths of the segments of the quasi-articulated structure according to where an object is grasped [7]. The use of this unique control space allows the octopus to control the rest of the fetching motion in intrinsic coordinates, similarly to certain types of human arm movements. Using these two control spaces greatly simplifies the complex requirement of overcoming the redundancy and carrying out inverse kinematic transformations in hyper-redundant structures [2]. Creating a stiffened but adjustable articulated structure (the joints can be generated anywhere along the arm) immensely reduces the number of variables that need to be controlled, i.e., from virtually infinite to only three degrees of freedom (DOFs). This dramatically simplifies the control of end-point movement while ensuring the high

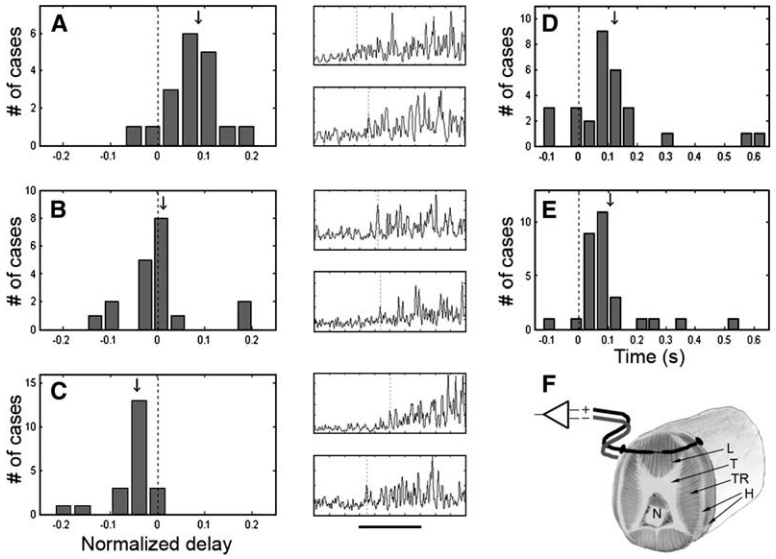

Figure 4. The Quasi-Articulated Structure Involves Two Waves of Muscle Contraction, which Propagate toward Each Other

(A) Histogram of the normalized delays between the onsets of the EMG signals recorded during a fetching movement by two electrodes in the proximal segment (n = 18).

(B and C) As in (A), but with the electrodes located at the medial joint (n = 19) and medial segment (n = 21), respectively. Onsets were calculated with the Generalized Likelihood Ratio algorithm and normalized according to the distance between electrodes. On the right of each histogram are examples of the rectified and filtered EMG signals recorded at the proximal (top) and distal (bottom) electrodes; the vertical lines represent the computed signal onsets. The scale bar represents 500 ms.

(D) Histogram showing a positive delay between the onset of the EMG signals and the onset of the medial-joint formation in movements in which the electrodes recorded from the proximal segment (L_1) (n = 29).

(E) As in (D), but the electrodes were located at the distal segment (L_2) (n = 29).

In all cases, the black arrows represent the average of each delay histogram.

(F) A scheme of the cross-section of an octopus arm, showing the muscular arrangement and the position of the electrodes. The following abbreviations are used: N, the arm's axial nerve cord; L, longitudinal muscle fibers; T, transverse muscle fibers; TR, trabecular bundles; and H, helical muscle fibers. The schematic position of the electrode inserted in the arm and the reference electrode are represented by the black and gray line curves, respectively. The thin area represents the region in which the wire electrode's insulation was removed.

accuracy required to achieve successful fetching movements.

As demonstrated by lesion experiments (Supplemental Data and Table S3), fetching movements differ from arm extension movements [22] in that higher brain areas are necessary for their execution. This, together with the invariant temporal pattern of joint formation (Figure S1) and the fact that two waves of muscle activation propagate in opposite directions along the arm (Figure 4), suggests the following scenario. A stimulus produced by the grasped object activates a peripheral mechanism, presumably via a high motor center in the brain. This mechanism consists of two waves of muscle contraction, which collide nearly midway along the arm, initiating or forming the medial joint. This scheme would be an efficient mechanism that drastically simplifies the computational needs for forming an object-dependent articulated structure.

These unique motor organization and control mechanisms immensely reduce the complexities associated with the generation of point-to-point movements with flexible arms. It is especially surprising that of all possible geometrical structures and motor control strategies with which a flexible arm can bring an object to the mouth, the octopus generates a quasi-articulated structure with a striking morphological and kinematic resemblance to the multijoint articulated limbs of vertebrates. Because the hypothetical common ancestor of cephalopods and vertebrates dates back to the beginning of Cambrian era (about 540 million years ago), fetching appears to be a genuine and rare case of evolutionary functional convergence, where two independent attributes (morphology and neural control) coevolved to achieve a common goal. We therefore suggest that the combination of a kinematically constrained articulated limb and a movement control strategy with simpler, more stereotypical movements in intrinsic coordinates offers an optimal solution for achieving precise point-to-point movements.

Supplemental Data

Supplemental Data include Supplemental Results and Discussion, Supplemental Experimental Procedures, five figures, and four tables and are available with this article online at: http://www.current-biology.com/cgi/content/full/16/8/767/DC1/.

Acknowledgments

This work was supported by Defense Advanced Research Projects Agency grant N66001-03-R-8043 and by the Israel Science Foundation grant 580/02. We thank Yoram Gutfreund for advice and critical reading, Jenny Kien for suggestions and editorial assistance, Tali Bdolah-Abram for statistical advice, and Yoram Yekutieli, Gilad Jacobson, Letizia Zullo, Michael Kuba, and the Smith Laboratory of the Hebrew University for their valuable help.

Received: September 27, 2005
Revised: February 7, 2006
Accepted: February 19, 2006
Published: April 17, 2006

References

1. Bernstein, N.A. (1967). The Coordination and Regulation of Movements (London: Pergamon).
2. Walker, I.D. (2000). Some issues in creating 'invertebrate' robots. International Symposium on Adaptive Motion of Animals and Machines, Montreal, Canada.
3. Flash, T., and Sejnowski, T.J. (2001). Computational approaches to motor control. Curr. Opin. Neurobiol. *11*, 655–662.
4. Sabes, P.N. (2000). The planning and control of reaching movements. Curr. Opin. Neurobiol. *10*, 740–746.
5. Wolpert, D.M., and Ghahramani, Z. (2000). Computational principles of movement neuroscience. Nat. Neurosci. *3* (*Suppl*), 1212–1217.
6. Flash, T., and Hochner, B. (2005). Motor primitives in vertebrates and invertebrates. Curr. Opin. Neurobiol. *15*, 660–666.

7. Sumbre, G., Fiorito, G., Flash, T., and Hochner, B. (2005). Motor control of flexible octopus arms. Nature *433*, 595–596.
8. Hollerbach, J.M. (1990). Planning of arm movements. In Visual Cognition and Action, D.N. Osherson, S.M. Kosslyn, and J.M. Hollerbach, eds. (Cambridge: MIT Press), pp. 183–211.
9. Lacquaniti, F., and Soechting, J.F. (1982). Coordination of arm and wrist motion during a reaching task. J. Neurosci. *2*, 399–408.
10. Kaminski, T., and Gentile, A.M. (1986). Joint control strategies and hand trajectories in multijoint pointing movements. J. Mot. Behav. *18*, 261–278.
11. Flanagan, J.R., and Ostry, D.J. (1989). Trajectories of human multijoint arm movements: Evidence of joint level planning. In Experimental Robotics I, Lecture Notes in Control and Information Sciences, Volume 139, V. Hayward and O. Khatib, eds. (Berlin: Springer-Verlag), pp. 594–613.
12. Liebermann, D. (1999). Intrinsic joint kinematic strategies for planning reaching and pointing movements towards 3-dimensional targets. PhD thesis, Weizmann Institute, Rehovot, Israel.
13. Malfait, N., Shiller, D.M., and Ostry, D.J. (2002). Transfer of motor learning across arm configurations. J. Neurosci. *22*, 9656–9660.
14. Ghafouri, M., Archambault, P.S., Adamovich, S.V., and Feldman, A.G. (2002). Pointing movements may be produced in different frames of reference depending on the task demand. Brain Res. *929*, 117–128.
15. Morasso, P. (1981). Spatial control of arm movements. Exp. Brain Res. *42*, 223–227.
16. Atkeson, C.G., and Hollerbach, J.M. (1985). Kinematic features of unrestrained vertical arm movements. J. Neurosci. *5*, 2318–2330.
17. Flash, T., and Henis, E. (1991). Arm trajectory modifications during reaching towards visual targets. J. Cogn. Neurosci. *3*, 220–230.
18. Berthier, N. (1996). Learning to reach: A mathematical model. Dev. Psychol. *32*, 811–823.
19. Rohrer, B., and Hogan, N. (2003). Avoiding spurious submovement decompositions: A globally optimal algorithm. Biol. Cybern. *89*, 190–199.
20. Rohrer, B., Fasoli, S., Krebs, H.I., Hughes, R., Volpe, B., Frontera, W.R., Stein, J., and Hogan, N. (2002). Movement smoothness changes during stroke recovery. J. Neurosci. *22*, 8297–8304.
21. Krebs, H.I., Aisen, M.L., Volpe, B.T., and Hogan, N. (1999). Quantization of continuous arm movements in humans with brain injury. Proc. Natl. Acad. Sci. USA *96*, 4645–4649.
22. Sumbre, G., Gutfreund, Y., Flash, T., Fiorito, G., and Hochner, B. (2001). Control of octopus arm extension by a peripheral motor program. Science *293*, 1845–1848.